HHS Public Access

Author manuscript

*Neuroimage*. Author manuscript; available in PMC 2022 March 01.

Published in final edited form as:

*Neuroimage*. 2022 March ; 248: 118866. doi:10.1016/j.neuroimage.2021.118866.

# High *b*-value diffusion tractography: Abnormal axonal network organization associated with medication-refractory epilepsy

**Ezequiel Gleichgerrcht**[a,*], **Simon S. Keller**[b,c], **Lorna Bryant**[b], **Hunter Moss**[d], **Tanja S. Kellermann**[a], **Shubhabrata Biswas**[c], **Anthony G. Marson**[b,c], **Janina Wilmskoetter**[a], **Jens H. Jensen**[d], **Leonardo Bonilha**[a]

[a]Department of Neurology, Medical University of South Carolina, Charleston, SC, USA

[b]Department of Pharmacology and Therapeutics, Institute of Systems, Molecular and Integrative Biology, University of Liverpool, UK

[c]The Walton Centre NHS Foundation Trust, Liverpool, UK

[d]Center for Biomedical Imaging, Medical University of South Carolina, Charleston, SC, USA

## Abstract

Diffusion magnetic resonance imaging (dMRI) tractography has played a critical role in characterizing patterns of aberrant brain network reorganization among patients with epilepsy. However, the accuracy of dMRI tractography is hampered by the complex biophysical properties of white matter tissue. High *b*-value diffusion imaging overcomes this limitation by better isolating axonal pathways. In this study, we introduce tractography derived from fiber ball imaging (FBI), a high *b*-value approach which excludes non-axonal signals, to identify atypical neuronal networks in patients with epilepsy. Specifically, we compared network properties obtained from multiple diffusion tractography approaches (diffusion tensor imaging, diffusion kurtosis imaging, FBI) in order to assess the pathophysiological relevance of network rearrangement in medication-responsive vs. medication-refractory adults with focal epilepsy. We show that drug-resistant epilepsy is associated with increased global network segregation detected by FBI-based tractography. We propose exploring FBI as a clinically feasible alternative to quantify topological changes that could be used to track disease progression and inform on clinical outcomes.

### Keywords

Diffusion; Magnetic resonance imaging; Fiber ball imaging; Tractography; Focal epilepsy



*Corresponding author. gleichge@musc.edu (E. Gleichgerrcht).

Author contributions

E. **Gleichgerrcht** : conceptualization, methodology, formal analysis, writing original draft; **S.S. Keller** : data curation, review and editing, project administration, funding acquisition; **L. Bryant:** data curation, project administration; **H. Moss** : data curation, formal analysis; **T. Kellermann** : formal analysis, investigation; **S. Biswas** : methodology; **A.G. Marson** : methodology; **J. Wilmskoetter** : formal analysis, visualization; **J.H. Jensen:** methodology, formal analysis, review and editing, supervision; **L. Bonilha** : conceptualization, methodology, formal analysis, writing original draft, supervision, funding.

## 1. Introduction

Epilepsy is a common neurological disorder defined by recurrent and unprovoked seizures (Sirven, 2015). It affects approximately 1% of the world's population and anti-seizure medications (ASM) are successful in completely controlling seizures in about 65% of epilepsy patients (Kwan et al., 2011; Tavakol et al., 2019). Unfortunately, 35% remain with poorly-controlled seizures despite ASM. The reasons seizures can-not be controlled with ASM for some patients remain mostly unknown.

Neuronal network architecture is central to the pathophysiology of epilepsy, since this disease affects not only specific brain regions, but also the interaction between multiple brain areas (Kramer and Cash, 2012). It has been recently hypothesized that epilepsy severity and clinical outcomes, e.g. ASM response, may be associated with more pronounced atypical patterns in brain network organization (Park et al., 2018; Tavakol et al., 2019). For this reason, the analytical evaluation of brain network properties is a promising approach for quantifying disease pathophysiology and could serve as a phenotypical marker.

Several quantitative neuroimaging studies have demonstrated that epilepsy is associated with brain atrophy and widespread cell loss (Galovic et al., 2019; Hatton et al., 2020; Lariviere et al., 2020; Winston et al., 2020). Patients with epilepsy typically exhibit atrophy affecting not only multiple gray matter structures, but also many white matter regions. Interestingly, axonal cell loss and white matter damage in epilepsy are associated with a paradoxical increment, at least in some areas, in regional network connectivity and network segregation properties.

Diffusion MRI tractography studies have demonstrated network rearrangement in epilepsy (Alizadeh et al., 2019; Bernhardt et al., 2013; Gleichgerrcht et al., 2021). Nonetheless, the accuracy of diffusion MRI tractography is hampered by the complex biophysical properties of white matter tissue. Complex white matter fiber anatomy, fiber crossings, heterogeneous peri-axonal milieu, and neuronal loss all impact the diffusion MRI signal and consequently affect the accuracy of fiber tracking (Savadjiev et al., 2008; Yeh et al., 2013). Thus, it remains unclear the degree to which network reorganization in epilepsy is related to abnormal topology of axonal projections. To resolve this issue, it is necessary to leverage newer approaches that improve tractography's accuracy to identify axonal projections and dissociate intra-axonal information from adjacent microstructure.

High *b*-value diffusion imaging is a promising new methodological development that combines improvements not only in MRI acquisition equipment (MR scanners) and sequence engineering, but also in mathematical modeling of diffusion data to yield increased accuracy in measuring tissue properties, hence enabling the characterization of intra-axonal and extra-neuronal components.

Specifically, fiber ball imaging (FBI) based tractography is a high *b*-value diffusion imaging approach in which the orientation distribution function (ODF) of water diffusion properties at each voxel is calculated based on intra-axonal signal alone, excluding the non-axonal signal that is commonly included in ODFs from other diffusion methods (Moss et al., 2019).

As such, FBI tractography can provide a more direct probe into neuronal networks and more accurately test the relationship between epilepsy and neuronal network reorganization.

In a recent epilepsy FBI study, we observed that refractory epilepsy is associated with abnormalities in white matter composition in comparison with patients with well controlled epilepsy and with healthy controls (Bryant et al., 2021). Patients with epilepsy demonstrated intra- and extra-axonal abnormalities suggesting alterations in axonal projections and peri-axonal milieu changes, respectively. Motivated by these tissue composition findings, we hypothesized that refractory epilepsy is associated with neuronal projection reorganization, i.e., changes in the configuration of axonal networks. Since FBI can provide a more specific evaluation of intra-axonal signal, we developed an FBI-based tractography approach to isolate axonal projection signal and to assess neuronal networks with higher accuracy. This study pioneers the use of FBI-derived tractography in epilepsy. We compared network properties obtained from multiple diffusion tractography approaches to assess the pathophysiological relevance of network rearrangement in patients with seizure control on ASM versus those with medication-refractory epilepsy.

## 2. Material and methods

### 2.1. Participants

We studied 14 healthy controls (age 38.5 ± 12.6, range 23–60 years old) and 29 patients diagnosed with focal epilepsy (age 39.4 ± 11.5, range 18–60 years old). Of these, 15 were drug-responsive, hereon referred to as well-controlled patients, while 14 adults with focal epilepsy had refractory epilepsy, hereon referred to as poorly-controlled patients. Patients with epilepsy were recruited from outpatient clinics and clinical databases from the Walton centre NHS Foundation Trust in Liverpool, UK. All patients and controls gave informed consent, and ethical approval was given by the Health Research Authority (IRAS project ID = 220,138; REC ID = 17/NW/0342).

All patients included in this cohort had clinical, neurophysiological, and/or radiographic features suggestive of focal epilepsy. The diagnosis was made by epileptologists based on seizure semiology and inter-ictal EEG recordings acquired in context of standard clinical care. Well-controlled patients had experienced no seizures for at least six months prior to recruitment into the study. Poorly-controlled (refractory) patients were experiencing persistent seizures prior to recruitment. Patients with primary generalized seizures, non-epileptic seizures, previous neurosurgery, or known progressive neurological disease were excluded from this study. A breakdown of all demographic and clinical information for patients is provided in Table 1.

Of note, the patients investigated in this study overlapped with the patients assessed in the recent Bryant et al. white matter tissue composition study by our group (2021). Despite such overlap, the prior study evaluated white matter compositional microstructure along tracts obtained from conventional diffusion fiber tracking, whereas the current study employs FBI-based tractography to assess resulting white matter network topological reconfigurations.

**2.1.1. MR acquisition—**All imaging data were acquired on a 3T Siemens Prisma MR scanner at the Liverpool Magnetic Resonance Imaging Center (LiM-RIC). Scanning included a T1-weighted magnetization-prepared rapid acquisition gradient echo sequence (MPRAGE; 192 slices, repetition time [TR] = 2000 ms, inversion time [TI] = 912 ms, echo time [TE] = 2.25 ms, resolution = 1.0 × 1.0 × 1.0 $mm^3$, flip angle = 8°, acquisition time = 7:30 min). An FBI sequence (TR = 4400 ms, TE = 100 ms, 46 axial slices, resolution = 2.7 × 2.7 × 2.7 $mm^3$, *b*-values = 0, 5000 $s/mm^2$, 128 directions) and a standard DKI scan (TR = 3200 ms, TE = 90 ms, 46 axial slices, resolution = 2.7 × 2.7 × 2.7 $mm^3$, *b*-values = 0, 1000, 2000$s/mm^2$, 60 directions) were also performed.

## 2.2. MR processing

For each subject, diffusion MRI data from all *b*-values acquired were concatenated and image preprocessing was performed using PyDesigner (Ades-Aron et al., 2018) (https://pydesigner.readthedocs.io/en/latest/). The preprocessing pipeline included denoising using a Marchenko-Pastur principal components analysis approach (Veraart et al., 2016), Gibbs ringing artifact correction (Kellner et al., 2016), eddy current correction (Andersson et al., 2016; Jenkinson et al., 2002), Gaussian kernel smoothing (Tabesh et al., 2011), and Rician noise bias correction (Gudbjartsson and Patz, 1995). For the preprocessed DKI data with $b = 0$, 1000, and 2000$s/mm^2$, Diffusional Kurtosis Estimator (DKE; https://www.nitric.org/projects.dke/ (Tabesh et al., 2011)) was applied to obtain both the diffusion and kurtosis tensors using both shells. A DTI ODF was determined from the diffusion tensor, and a DKI ODF was determined from the diffusion and kurtosis tensors, as previously described (Glenn et al., 2016). The FBI ODFs were obtained from the 5000 $s/mm^2$ *b*-value images by employing an inverse generalized Funk transform with the reference diffusivity scale $D_0$ set to 3.0 $\mu m^2/ms$ (Jensen et al., 2016; McKinnon et al., 2018; Moss and Jensen, 2021; Moss et al., 2019).

The ODFs from each diffusion MRI approach (DTI, DKI and FBI) were encoded as .fib files and whole-brain deterministic white matter fiber tractography, with fiber directions being obtained from the respective ODF peaks, was then performed using an Euler algorithm with in-house MATLAB scripts with 100,000 identical seed points across diffusion methods, cutoff of FA less than 0.1, an angular threshold of 35°, step size 0.1 mm, and a minimum track length of 30 mm. The resultant white matter fiber tractography files (.trk) were then normalized to standard Montreal Neurological Institute (MNI) space using SPM8 (Greve and Fischl, 2009; Jenkinson and Smith, 2001) and the MNI FA template. Final white matter fiber tractography was then analyzed using DSI Studio (http://dsi-studio.labsolver.org).

## 2.3. Connectome reconstruction and whole brain network properties

Whole brain connectivity matrices (connectomes) were obtained from all participants. MNI normalized whole brain tractography .trk files from each modality were imported into the software package DSI-studio, which was used to calculate the connectivity matrix between all gray matter regions belonging to the AAL2 parcellation atlas. The connectivity matrix was calculated by assessing the number of tracts passing two ROIs, normalized by the sum of the inverse of the length of their connections (“ncount2”). The resulting weighted connectivity matrix was binarized using DSI-studio’s connectivity threshold of 0.001.

Whole brain graph theory network properties were obtained from each binarized connectome using DSI-Studio's network measures function, which employs measures from the brain connectivity toolbox (https://sites.google.com/site/bctnet/). In this study, we focused on 3 specific biologically relevant global network measures that have been extensively used in epilepsy: **global density** (which reflects the number of connections across all ROIs), **global clustering coefficient** (which reflects the number of connections between neighbors of a given ROI, with higher values indicating higher network segregation) and **efficiency** (which indicates the inverse of path length between pairs of ROIs, with higher values indicating higher network efficiency and higher network integration). Of note, other commonly used graph theory measures in epilepsy such as betweenness or page-rank centrality are considered to be more relevant as measures of regional network properties and were hence not assessed here since the goal was to evaluate global network properties.

Fig. 1 provides a summary of the image processing pipeline used in this study.

To evaluate differences in location or numbers of fibers identified by each diffusion modality, we examined the mean tract density values in white matter regions of interest (ROIs) from the NatBrainLab atlas.

To evaluate whether global network properties could be explained by preferential changes in short-range vs. long-range fiber proportions in each group, we measured the ratio of short/long ratio of fibers per individual. To define short and range pathways, the Euclidean distance between each AAL2 ROI pair was calculated, and fibers located in the connections for the lower Euclidean distance quartile were considered the short-range group, whereas fibers in connections for the highest quartile were considered the long-range group.

## 2.4. Statistical analyses

**2.4.1. Regional differences in fiber tracking related to each modality—**To avoid confounders related to epilepsy, we assessed only numbers obtained from controls, and we examined differences between modalities for each white matter ROI using one-way Analysis of Variance (ANOVA) (within-subjects factor: DTI vs. DKI vs. FBI).

**2.4.2. Fiber length and epilepsy—**We compared the ratio of short/long fibers using a one-way ANOVA with subject group set as the between-subject factor (short/long fibers in controls vs. patients and well-controlled vs. poorly-controlled patients).

We also assessed whether there was a relationship between the difference in the number of fibers tracked with each modality and the distance travelled by the fibers. This was accomplished by performing a Pearson correlation analysis between: 1) the ratio of fiber counts from one modality relative to another (for example, FBI over DTI) for each connectome link, and 2) the Euclidian distance of the gray matter ROIs in that link.

**2.4.3. Global network properties—**We computed 3 global network measures for every participant across the 3 types of diffusion, as described above: global network density, global network efficiency, and global network clustering coefficient. For each measure,

a repeated measures analysis of variance (ANOVA) was used to evaluate the effects of diffusion (within-subjects factor: DTI vs. DKI vs. FBI) and subject group (between-subjects factor: controls vs. patients with seizures well controlled with ASM vs. patients with seizures poorly controlled with ASM).

## 3. Results

### 3.1. Demographics and clinical variables

There were no significant differences in the proportion of female- to-male participants between controls (7:7) and patients (16:15) ($\chi^2 = 0.10$, $p = 0.75$) or between well- (8:7) and poorly-controlled (8:6) patients ($\chi^2 = 0.04$, $p = 0.84$). The mean age of controls (38.1 ± 13.0 years) and patients with epilepsy (39.7 ± 11.8) was not significantly different ($t_{41} = 0.38$, $p = 0.71$). Similarly, no significant differences were found for age ($t_{41} = 0.5$, $p = 0.62$) between the two groups of patients (well-controlled 40.7 ± 12.1 years vs. poorly-controlled 38.5 ± 12.0 years).

### 3.2. Diffusion tractography and connectome reconstruction

Fig. 2 demonstrates the ODFs for each diffusion modality. The whole brain tract-density imaging for one representative subject obtained with each diffusion is also shown in Fig. 2. The group-average connectomes obtained from each diffusion modality is shown in Fig. 3.

**3.2.1. Regional differences in fiber tracking related to each modality—**FBI was able to identify more fibers compared with DKI, which, in turn, identified more fibers compared with DTI. Fig. 4 demonstrates where and how much each modality differed in terms of fiber tracking. The majority of the white matter ROIs had more fibers resolved with FBI compared with DKI or DTI. These are shown in Fig. 5.

### 3.3. Fiber length and subject groups

The number of fibers in relationship with connectome link distance is shown in Fig. 6. There was not a relationship between distance and the number of additional fibers tracked by each modality (FBI vs DTI, $R = 0.002$, $p = 0.85$; DKI vs DTI $R = 0.001$, $p = 0.88$), indicating that the fiber tracking benefits of FBI or DKI were not dependent on fiber length.

We did not observe a significant difference between groups in the ratio of short/long fibers with each modality (DTI $F(2,42) = 0.236$, $p = 0.791$; DKI $F(2,42) = 0.243$, $p = 0.786$; DKI $F(2,42) = 0.411$, $p = 0.67$).

### 3.4. Whole brain network properties

**3.4.1. Global density—**The Mauchly's Test of Sphericity was significant, $Chi^2$ (2) = 32,735, $p < 0.001$. The results of the repeated measures ANOVA with Greenhouse-Geisser correction revealed a significant main effect of diffusion modality on global density ($F(2, 80) = 174.97$, $p < 0.001$, $\eta p^2 = 0.814$). Global density was lowest for DTI (Mean ± SE = 0.135 ± 0.002), followed by DKI (0.149 ± 0.002), and highest with FBI (0.183 ± 0.004).

There was no main effect of controls vs. patient groups for global density (controls = 0.159 ± 0.004, patients [well-controlled] = 0.149 ± 0.004, patients [poorly-controlled] = 0.158 ± 0.004), $F(2, 40) = 1.76$, $p = 0.19$, $\eta p^2 = 0.08$).

There was not a significant interaction between diffusion modality and group ($F(4, 80) = 0.67$, $p = 0.582$, $\eta p^2 = 0.029$) (Fig. 7).

**3.4.2. Global efficiency—**The Mauchly's Test of Sphericity was significant, $Chi^2$ (2) = 25.10, $p < 0.001$. The results of the repeated measures ANOVA with Greenhouse-Geisser correction revealed a significant main effect of diffusion modality on global density ($F(2, 80) = 170.16$, $p < 0.001$, $\eta p^2 = 0.810$). Global efficiency was lowest for DTI (Mean ± SE = 0.509 ± 0.002), followed by DKI (0.527 ± 0.002), and highest with FBI (0.555 ± 0.004).

There was no main effect of controls vs. patient groups for global density (controls = 0.534 ± 0.003, patients [well-controlled] = 0.526 ± 0.003, patients [poorly-controlled] = 0.531 ± 0.003), $F(2, 40) = 1.987$, $p = 0.15$, $\eta p^2 = 0.09$).

There was not a significant interaction between diffusion modality and group ($F(4, 80) = 0.47$, $p = 0.98$, $\eta p^2 = 0.029$) (Fig. 7).

**3.4.3. Global clustering coefficient—**The Mauchly's Test of Sphericity was not significant $Chi^2 = 2.13$, $p = 0.345$. The results of the repeated measures ANOVA revealed a significant main effect of diffusion modality on global clustering coefficient ($F(2, 80) = 22.19$, $p < 0.001$, $\eta p^2 = 0.36$). Global clustering coefficient was lowest for DKI (Mean ± SE = 0.546 ± 0.004), followed by DTI (0.538 ± 0.004), and highest with FBI (0.557 ± 0.003).

There was no main effect of controls vs. patient groups for global clustering coefficient (controls = 0.547 ± 0.006, patients [well-controlled] = 0.542 ± 0.006, patients [poorly-controlled] = 0.552 ± 0.006), $F(2, 40) = 0.83$, $p = 0.46$, $\eta p^2 = 0.39$).

We found a significant interaction between diffusion modality and group ($F(4, 80) = 2.82$, $p = 0.031$, $\eta p^2 = 0.12$) such that the difference in density between controls and patients (poorly-controlled) was most pronounced in FBI, $T(26) = 2.596$, $p = 0.015$ (Fig. 7).

## 4. Discussion

In this study, we tested the hypothesis that epilepsy is associated with global network reorganization in the form of increased regional segregation by comparing whole brain tractography connectivity maps using different diffusion modalities. We confirmed our hypothesis, while demonstrating that high *b*-value diffusion imaging, i.e., FBI, is sensitive to epilepsy related changes, particularly in the group of patients whose seizures were not controlled with medication. Taken together, the results of this study suggest that FBI fiber tractography may be more sensitive than conventional DTI tractography in assessing changes in microstructure associated with refractory epilepsy. This is likely because DTI tractography is degraded by signal from extra-axonal water while FBI tractography is not. These findings have implications regarding the pathophysiology of epilepsy, as well as

the potential use of high *b*-value diffusion imaging in epilepsy and other neurological conditions. These are discussed below.

### 4.1. Atypical neuronal network associated epilepsy

Multiple studies have demonstrated white matter volume atrophy and microstructural changes in white matter associated with epilepsy (Deleo et al., 2018; Hatton et al., 2020; Lin et al., 2020; Rodriguez-Cruces and Concha, 2015). The microstructural changes most commonly observed were markers of cell loss such as reduction in fractional anisotropy or increment in mean diffusivity (Concha et al., 2009; McDonald et al., 2008), using conventional single- or multi-shell diffusion MRI. Paradoxically, in spite of cell loss associated with epilepsy, fiber tracking studies have also demonstrated increased segregation measures (van Diessen et al., 2014), which may indicate network reorganization of imbalanced cell loss affecting more prominently cells associated with network integration. Even with the expected reduction in connectivity due to fewer axonal projections, epilepsy is associated with an atypical network architecture in the form of strengthening of regional connectivity.

Atypical neuronal network architecture in epilepsy is possibly caused by abnormal plasticity, where seizure recurrence is associated with increased co-activation of neurons within the epileptogenic pathways, leading to regional connectivity strengthening and increased network segregation (Scharfman, 2007; van Diessen et al., 2014). Importantly, this is possibly a shared phenomenon across different forms of epilepsy, as suggested by the data described in this study. Across multiple forms of epilepsy, different regions are associated with seizure onset and ictal maintenance, and therefore regional properties depend on the epilepsy type. Nonetheless, global network abnormalities are possibly a common denominator across multiple epilepsy types when seizures are not well-controlled with medication.

In this study, we did not observe a difference in the ratio of long and short fibers in patients compared with controls. Only a small sample was evaluated, and this negative result may be related to power (see limitations section below). Nonetheless, this is an important observation, since network abnormalities in segregation and integration could theoretically be related to a preferential damage in long-range vs. short-range fibers. For instance, the preferential damage in long-range fibers could lead to reduced efficiency, reduced integration and atypical segregation patterns. The short/long fiber ratio is particularly relevant in neurology since premature aging and small vessel disease from cardiovascular risk factors can preferentially affect long-range fibers and disrupt network topology (Marebwa et al., 2018). While epilepsy may be associated with premature brain aging as well (Hermann et al., 2008), it remains to be determined if similar mechanisms related to short/long fiber abnormalities contribute to its pathophysiology, particularly among more specific forms of focal epilepsy.

### 4.2. High b-value imaging

This study pioneered the use of FBI-based tractography in epilepsy. FBI leverages innovations in MR scanner hardware and sequence engineering, as well as mathematical

modeling of the diffusion signal, in order to improve the accuracy of tracking axonal projections (Jensen et al., 2016; Moss et al., 2019). The regional differences in FBI fiber tracking are readily apparent not only in regions with predominantly unidirectional anisotropic signal, e.g., corpus callosum, but also in areas with significant fiber crossing. For instance, for the same representative subject shown in Fig. 1, the number of additional fibers tracked in each region for FBI in comparison with DKI and DTI are shown in Fig. 4. Note that DKI already provided additional fiber tracking fidelity compared with DTI (Glenn et al., 2016), which is further improved with FBI. FBI not only provides enhanced fiber tracking for multiple brain regions but, more importantly, can resolve fibers in multiple white matter regions in which DTI and DKI are not able to identify fiber projections. This difference in also apparent in Fig. 4. The evidence supporting the hypothesis that strong diffusion weightings can be used to suppress the contribution from extra-axonal water is that the direction-averaged dMRI signal decays in white matter as 1/sqrt($b$) for $b$-values exceeding about 4000 s/mm$^2$. In fact, this has been verified for b-values anywhere from 10,000 s/mm$^2$ (Moss et al., 2019) to 25,000 s/mm$^2$ (Veraart et al., 2019, 2020).

A key aspect of FBI, and some other high $b$-value diffusion imaging methods, is that the MRI signal originates predominately from intra-axonal water since the signal from the more mobile pool of extra-axonal water is suppressed by strong diffusion weighting (Bryant et al., 2021; Jensen et al., 2016). As a consequence, FBI fiber tractography solely reflects the geometry of axons without contamination from the extra-axonal microenvironment, resulting in improved fidelity and robustness with respect to tissue changes (e.g., edema) that might otherwise impact the estimated axonal pathways. In contrast, both DTI and DKI fiber tractography rely on MRI signals emanating from a mixture of both intra-axonal and extra-axonal water, which can lower their accuracy and reliability (Fieremans et al., 2011). This distinction between FBI relative to DTI and DKI fiber tractography can be more precisely expressed by saying that FBI tractography is based on a “fiber ODF”, which provides the angular density of axon orientations, while DTI and DKI, as well as a number of other popular techniques including q-ball imaging and diffusion spectrum imaging, are based on “diffusion ODFs”, which instead indicate preferred directions of water diffusion (Dell’Acqua and Tournier, 2019).

FBI also has advantages in comparison to alternative methods that utilize fiber ODFs, such as constrained spherical deconvolution (Tournier et al., 2004) and Richardson-Lucy spherical deconvolution (Dell’Acqua and Tournier, 2019), in that the ODF is calculated from a simple linear transformation of the raw diffusion data without the need for regularization or other complex numerical procedures. In addition, FBI does not require a globally defined response function so the ODF in each voxel is determined entirely with information from that voxel. Constrained spherical deconvolution, in contrast, typically employs a response function that is obtained from measurements in regions with high fractional anisotropy and then applied throughout the brain to calculate the ODF; as a consequence, the ODF is not based solely on local information which could be problematic in subjects with heterogeneous brain pathology. Ideally, future studies would be able to correlate the diffusion metrics derived from FBI with histopathological observations of fiber density and configuration in order to confirm the mechanism underlying these radiographic advantages.

### 4.3. Limitations

This is a pioneering proof-of-concept study to assess the utility of FBI based tractography in epilepsy. As such, the number of patients included in this study is small. Moreover, the patient population was composed of consecutive individuals with various epilepsy syndromes and the sample is hence quite heterogeneous. Thus, syndrome-specific changes could not be further investigated. It would also be important to determine whether the advantages of FBI tractography generalize across age groups, sex/gender, race/ethnic groups, etc. Of note, exploring regional/local topological features such as hubness, integration, and centrality was not feasible in this study since different regions were implicated across patients. Subsequent cohorts with larger sample sizes and more homogeneous cohorts will be critical in exploring local topological properties with FBI. Moreover, there are relevant potential confounders that are worth studying as they relate to FBI changes; in other words, in determining whether they are related to structural network changes detected by FBI but not by other diffusion approaches with lower *b*-values. Some of these will require a larger cohort to allow for between-group comparisons, such as the manifestation of specific seizure semiologies (e.g. the presence or absence of FBTC seizures), while others will benefit from longitudinal acquisition of diffusion data at different time points (e.g. the role of duration of epilepsy in structural network changes).

We note that we used binarized connectomes in this study since we were mainly concerned with understanding the topological patterns of connections between nodes, irrespective of variations in their weights, since the latter could further be influenced by the diffusion type. This is important, since variations in certain topological features of weighted matrices are often difficult to disentangle from variations in the weights themselves (e.g. van Wijk et al., 2010). However, it will be critical for future studies to also compare the performance of weighted matrices across diffusion techniques.

The major limitation of FBI is that it requires high *b*-value (i.e. > 4000 s/mm$^2$) diffusion MRI data in order to adequately suppress the extra-axonal signal, which reduces the signal-to-noise ratio relative to lower *b*-value methods such as DTI and DKI. To compensate, FBI typically necessitates the use of somewhat larger voxels than either DTI or DKI. In addition, about 60 or more diffusion directions are needed for FBI (Moss et al., 2019), which is substantially larger than the minimum number needed for DTI (6 directions) and DKI (15 directions) resulting in longer minimal scan times. However, the latest generation of clinical MRI scanners, with strong field gradients of about 80 mT/m, greatly increase the practicality of FBI. It must be noted that FBI has only been tested on 3T scanners, and its feasibility for other field levels remains to be established. In terms of generalizability, the software needed to process FBI has been recently described (Dhiman et al., 2021) and is freely available at https://github.com/m-ama.

## 5. Conclusions

High *b*-value diffusion imaging can better isolate axonal pathways and identify core pathophysiological neuronal networks associated with epilepsy. Medication-refractory epilepsy is associated with increased global network segregation, which is a quantifiable topological change that could be used to track disease progression and inform on clinical

outcomes. FBI based tractography is a clinically feasible high *b*-value diffusion imaging method that may be more sensitive to alterations in brain structural connectivity than conventional the fiber tracking approaches based on DTI and DKI.

## Funding

This work was supported by a grant from the National Institute of Neurological Disorders and Stroke (NINDS) 1R01NS110347-01A to Leonardo Bonilha and Jens Jensen as well as a UK Medical Research Council (MRC) DiMeN Doctoral Training Partnership Studentship awarded to Lorna Bryant and MRC grants awarded to Simon S. Keller (MR/S00355X/1 and MR/K023152/1).

## Data and code availability statement

The data for this study is available through a request to the corresponding author.

All computational software described in the Methods section is open source and available to all audiences through their corresponding download sites.

## Glossary

| | |
|---|---|
| **DTI** | diffusion tensor imaging |
| **DKI** | diffusion kurtosis imaging |
| **FBI** | fiber ball imaging |

## References

Ades-Aron B, Veraart J, Kochunov P, McGuire S, Sherman P, Kellner E, Novikov DS, Fieremans E, 2018. Evaluation of the accuracy and precision of the diffusion parameter EStImation with Gibbs and NoisE removal pipeline. Neuroimage 183, 532–543. [PubMed: 30077743]

Alizadeh M, Kozlowski L, Muller J, Ashraf N, Shahrampour S, Mohamed FB, Wu C, Sharan A, 2019. Hemispheric regional based analysis of diffusion tensor imaging and diffusion tensor tractography in patients with temporal lobe epilepsy and correlation with patient outcomes. Sci. Rep 9, 215. [PubMed: 30659215]

Andersson JLR, Graham MS, Zsoldos E, Sotiropoulos SN, 2016. Incorporating outlier detection and replacement into a non-parametric framework for movement and distortion correction of diffusion MR images. Neuroimage 141, 556–572. [PubMed: 27393418]

Bernhardt BC, Hong S, Bernasconi A, Bernasconi N, 2013. Imaging structural and functional brain networks in temporal lobe epilepsy. Front. Hum. Neurosci 7, 624. [PubMed: 24098281]

Bryant L, McKinnon ET, Taylor JA, Jensen JH, Bonilha L, de Bezenac C, Kreilkamp BAK, Adan G, Wieshmann UC, Biswas S, Marson AG, Keller SS, 2021. Fiber ball white matter modeling in focal epilepsy. Hum. Brain Mapp

Concha L, Beaulieu C, Collins DL, Gross DW, 2009. White-matter diffusion abnormalities in temporal-lobe epilepsy with and without mesial temporal sclerosis. J. Neurol. Neurosurg. Psychiatry 80, 312–319. [PubMed: 18977826]

Deleo F, Thom M, Concha L, Bernasconi A, Bernhardt BC, Bernasconi N, 2018. Histological and MRI markers of white matter damage in focal epilepsy. Epilepsy Res 140, 29–38. [PubMed: 29227798]

Dell'Acqua F, Tournier JD, 2019. Modelling white matter with spherical deconvolution: how and why? NMR Biomed 32, e3945. [PubMed: 30113753]

Dhiman S, Teves JB, Thorn KE, McKinnon ET, Moss HG, Adisetiyo V, Ades-Aron B, Veraart J, Chen J, Fieremans E, Benitez A, Helpern JA, Jensen JH, 2021. PyDesigner: a pythonic

implementation of the DESIGNER pipeline for diffusion tensor and diffusional kurtosis imaging. bioRxiv 2021.10.20.465189.

Fieremans E, Jensen JH, Helpern JA, 2011. White matter characterization with diffusional kurtosis imaging. Neuroimage 58, 177–188. [PubMed: 21699989]

Galovic M, van Dooren VQH, Postma T, Vos SB, Caciagli L, Borzi G, Rosillo JC, Vuong KA, de Tisi J, Nachev P, Duncan JS, Koepp MJ, 2019. Progressive cortical thinning in patients with focal epilepsy. JAMA Neurol.

Gleichgerrcht E, Greenblatt AS, Kellermann TS, Rowland N, Vandergrift WA, Edwards J, Davis KA, Bonilha L, 2021. Patterns of seizure spread in temporal lobe epilepsy are associated with distinct white matter tracts. Epilepsy Res 171, 106571. [PubMed: 33582534]

Glenn GR, Jensen JH, Helpern JA, Spampinato MV, Kuzniecky R, Keller SS, Bonilha L, 2016. Epilepsy-related cytoarchitectonic abnormalities along white matter pathways. J. Neurol. Neurosurg. Psychiatry 87, 930–936. [PubMed: 27076491]

Greve DN, Fischl B, 2009. Accurate and robust brain image alignment using boundary-based registration. Neuroimage 48, 63–72. [PubMed: 19573611]

Gudbjartsson H, Patz S, 1995. The Rician distribution of noisy MRI data. Magn. Reson. Med 34, 910–914. [PubMed: 8598820]

Hatton SN, Huynh KH, Bonilha L, Abela E, Alhusaini S, Altmann A, Alvim MKM, Balachandra AR, Bartolini E, Bender B, Bernasconi N, Bernasconi A, Bernhardt B, Bargallo N, Caldairou B, Caligiuri ME, Carr SJA, Cavalleri GL, Cendes F, Concha L, Davoodi-Bojd E, Desmond PM, Devinsky O, Doherty CP, Domin M, Duncan JS, Focke NK, Foley SF, Gambardella A, Gleichgerrcht E, Guerrini R, Hamandi K, Ishikawa A, Keller SS, Kochunov PV, Kotikalapudi R, Kreilkamp BAK, Kwan P, Labate A, Langner S, Lenge M, Liu M, Lui E, Martin P, Mascalchi M, Moreira JCV, Morita-Sherman ME, O'Brien TJ, Pardoe HR, Pariente JC, Ribeiro LF, Richardson MP, Rocha CS, Rodriguez-Cruces R, Rosenow F, Severino M, Sinclair B, Soltanian-Zadeh H, Striano P, Taylor PN, Thomas RH, Tortora D, Velakoulis D, Vezzani A, Vivash L, von Podewils F, Vos SB, Weber B, Winston GP, Yasuda CL, Zhu AH, Thompson PM, Whelan CD, Jahanshad N, Sisodiya SM, McDonald CR, 2020. White matter abnormalities across different epilepsy syndromes in adults: an ENIG-MA-Epilepsy study. Brain 143, 2454–2473. [PubMed: 32814957]

Hermann B, Seidenberg M, Sager M, Carlsson C, Gidal B, Sheth R, Rutecki P, Asthana S, 2008. Growing old with epilepsy: the neglected issue of cognitive and brain health in aging and elder persons with chronic epilepsy. Epilepsia 49, 731–740. [PubMed: 18031544]

Jenkinson M, Bannister P, Brady M, Smith S, 2002. Improved optimization for the robust and accurate linear registration and motion correction of brain images. Neuroimage 17, 825–841. [PubMed: 12377157]

Jenkinson M, Smith S, 2001. A global optimisation method for robust affine registration of brain images. Med. Image Anal 5, 143–156. [PubMed: 11516708]

Jensen JH, Russell Glenn G, Helpern JA, 2016. Fiber ball imaging. Neuroimage 124, 824–833. [PubMed: 26432187]

Kellner E, Dhital B, Kiselev VG, Reisert M, 2016. Gibbs-ringing artifact removal based on local subvoxel-shifts. Magn. Reson. Med 76, 1574–1581. [PubMed: 26745823]

Kramer MA, Cash SS, 2012. Epilepsy as a disorder of cortical network organization. Neuroscientist 18, 360–372. [PubMed: 22235060]

Kwan P, Schachter SC, Brodie MJ, 2011. Drug-resistant epilepsy. N Engl. J. Med 365, 919–926. [PubMed: 21899452]

Lariviere S, Rodriguez-Cruces R, Royer J, Caligiuri ME, Gambardella A, Concha L, Keller SS, Cendes F, Yasuda C, Bonilha L, Gleichgerrcht E, Focke NK, Domin M, von Podewills F, Langner S, Rummel C, Wiest R, Martin P, Kotikalapudi R, O'Brien TJ, Sinclair B, Vivash L, Desmond PM, Alhusaini S, Doherty CP, Cavalleri GL, Delanty N, Kalviainen R, Jackson GD, Kowalczyk M, Mascalchi M, Semmelroch M, Thomas RH, Soltanian-Zadeh H, Davoodi-Bojd E, Zhang J, Lenge M, Guerrini R, Bartolini E, Hamandi K, Foley S, Weber B, Depondt C, Absil J, Carr SJA, Abela E, Richardson MP, Devinsky O, Severino M, Striano P, Tortora D, Hatton SN, Vos SB, Duncan JS, Whelan CD, Thompson PM, Sisodiya SM, Bernasconi A, Labate A, McDonald CR, Bernasconi N, Bernhardt BC, 2020. Network-based atrophy modeling in the common epilepsies: a worldwide ENIGMA study. Sci. Adv 6.

Lin H, Leng X, Qin C, Wang W, Zhang C, Qiu S, 2020. Altered white matter structural network in frontal and temporal lobe epilepsy: a graph-theoretical study. Front. Neurol 11, 561. [PubMed: 32625164]

Marebwa BK, Adams RJ, Magwood GS, Basilakos A, Mueller M, Rorden C, Fridriksson J, Bonilha L, 2018. Cardiovascular risk factors and brain health: impact on long-range cortical connections and cognitive performance. J. Am. Heart Assoc 7, e010054. [PubMed: 30520672]

McDonald CR, Ahmadi ME, Hagler DJ, Tecoma ES, Iragui VJ, Gharapetian L, Dale AM, Halgren E, 2008. Diffusion tensor imaging correlates of memory and language impairments in temporal lobe epilepsy. Neurology 71, 1869–1876. [PubMed: 18946001]

McKinnon ET, Helpern JA, Jensen JH, 2018. Modeling white matter microstructure with fiber ball imaging. Neuroimage 176, 11–21. [PubMed: 29660512]

Moss HG, Jensen JH, 2021. Optimized rectification of fiber orientation density function. Magn. Reson. Med 85, 444–455. [PubMed: 32710476]

Moss HG, McKinnon ET, Glenn GR, Helpern JA, Jensen JH, 2019. Optimization of data acquisition and analysis for fiber ball imaging. Neuroimage 200, 690–703. [PubMed: 31284026]

Park KM, Lee BI, Shin KJ, Ha SY, Park J, Kim TH, Mun CW, Kim SE, 2018. Progressive topological disorganization of brain network in focal epilepsy. Acta Neurol. Scand 137, 425–431. [PubMed: 29344935]

Rodriguez-Cruces R, Concha L, 2015. White matter in temporal lobe epilepsy: clinico–pathological correlates of water diffusion abnormalities. Quant. Imaging Med. Surg 5, 264–278. [PubMed: 25853084]

Savadjiev P, Campbell JS, Descoteaux M, Deriche R, Pike GB, Siddiqi K, 2008. Labeling of ambiguous subvoxel fibre bundle configurations in high angular resolution diffusion MRI. Neuroimage 41, 58–68. [PubMed: 18367409]

Scharfman HE, 2007. The neurobiology of epilepsy. Curr. Neurol. Neurosci. Rep 7, 348–354. [PubMed: 17618543]

Sirven JI, 2015. Epilepsy: a spectrum disorder. Cold Spring Harb. Perspect. Med 5, a022848. [PubMed: 26328931]

Tabesh A, Jensen JH, Ardekani BA, Helpern JA, 2011. Estimation of tensors and tensor-derived measures in diffusional kurtosis imaging. Magn. Reson. Med 65, 823–836. [PubMed: 21337412]

Tavakol S, Royer J, Lowe AJ, Bonilha L, Tracy JI, Jackson GD, Duncan JS, Bernasconi A, Bernasconi N, Bernhardt BC, 2019. Neuroimaging and connectomics of drug-resistant epilepsy at multiple scales: from focal lesions to macroscale networks. Epilepsia 60, 593–604. [PubMed: 30889276]

Tournier JD, Calamante F, Gadian DG, Connelly A, 2004. Direct estimation of the fiber orientation density function from diffusion-weighted MRI data using spherical deconvolution. Neuroimage 23, 1176–1185. [PubMed: 15528117]

van Diessen E, Zweiphenning WJ, Jansen FE, Stam CJ, Braun KP, Otte WM, 2014. Brain network organization in focal epilepsy: a systematic review and meta–analysis. PLoS One 9, e114606. [PubMed: 25493432]

van Wijk BC, Stam CJ, Daffertshofer A, 2010. Comparing brain networks of different size and connectivity density using graph theory. PLoS One 5, e13701. [PubMed: 21060892]

Veraart J, Fieremans E, Novikov DS, 2019. On the scaling behavior of water diffusion in human brain white matter. Neuroimage 185, 379–387. [PubMed: 30292815]

Veraart J, Novikov DS, Christiaens D, Ades-Aron B, Sijbers J, Fieremans E, 2016. Denoising of diffusion MRI using random matrix theory. Neuroimage 142, 394–406. [PubMed: 27523449]

Veraart J, Nunes D, Rudrapatna U, Fieremans E, Jones DK, Novikov DS, Shemesh N, 2020. Nonivasive quantification of axon radii using diffusion MRI. Elife 9.

Winston GP, Vos SB, Caldairou B, Hong SJ, Czech M, Wood TC, Wastling SJ, Barker GJ, Bernhardt BC, Bernasconi N, Duncan JS, Bernasconi A, 2020. Microstructural imaging in temporal lobe epilepsy: diffusion imaging changes relate to reduced neurite density. Neuroimage Clin 26, 102231. [PubMed: 32146320]

Yeh FC, Verstynen TD, Wang Y, Fernandez-Miranda JC, Tseng WY, 2013. Deterministic diffusion fiber tracking improved by quantitative anisotropy. PLoS One 8, e80713. [PubMed: 24348913]

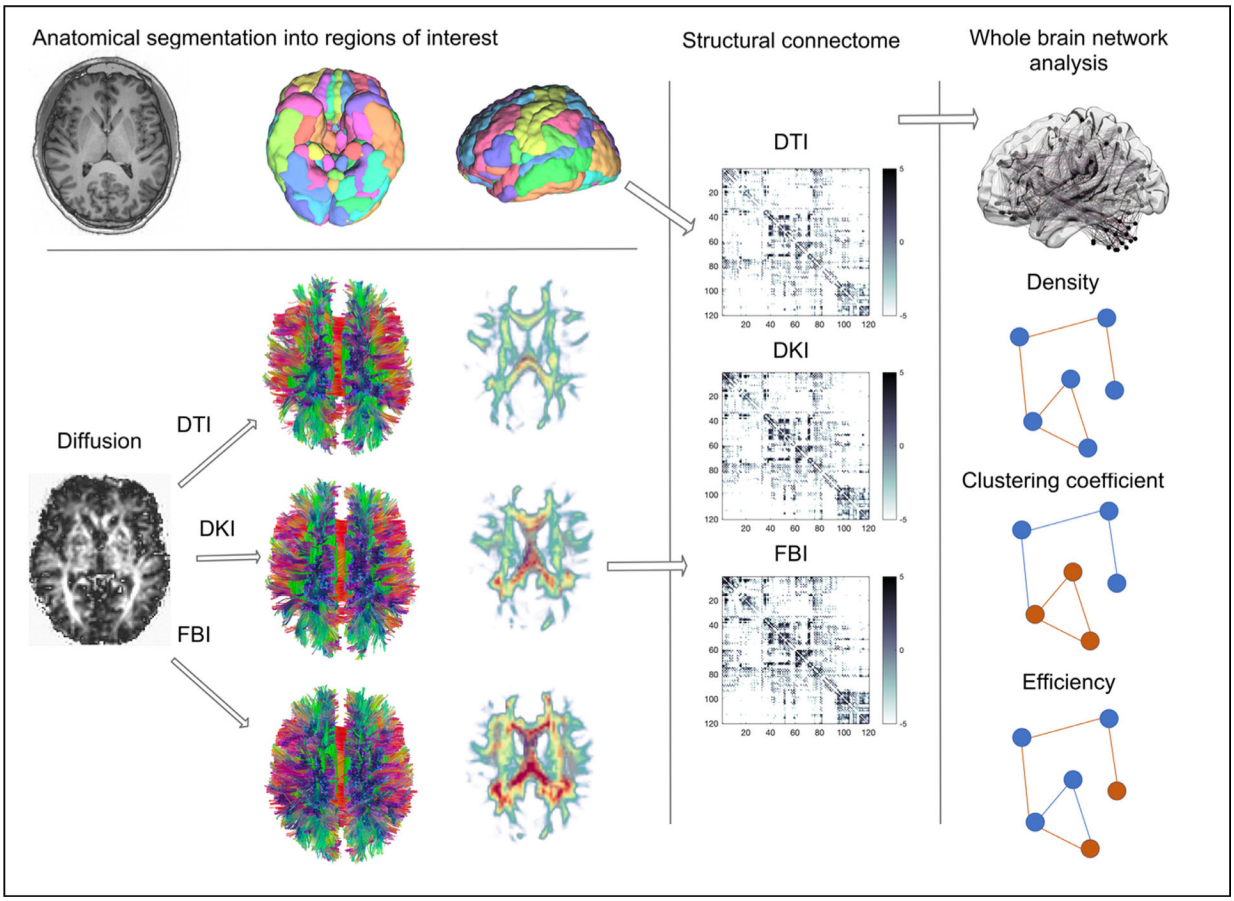


**Fig. 1. –.**

The image processing pipeline used in this study. Whole brain DTI tractography, DKI tractograpy and FBI tractography were reconstructed (the axial slices demonstrate tract density images), from which whole brain connectomes were obtained. Three global network properties were analyzed (density, efficiency and clustering coefficient).

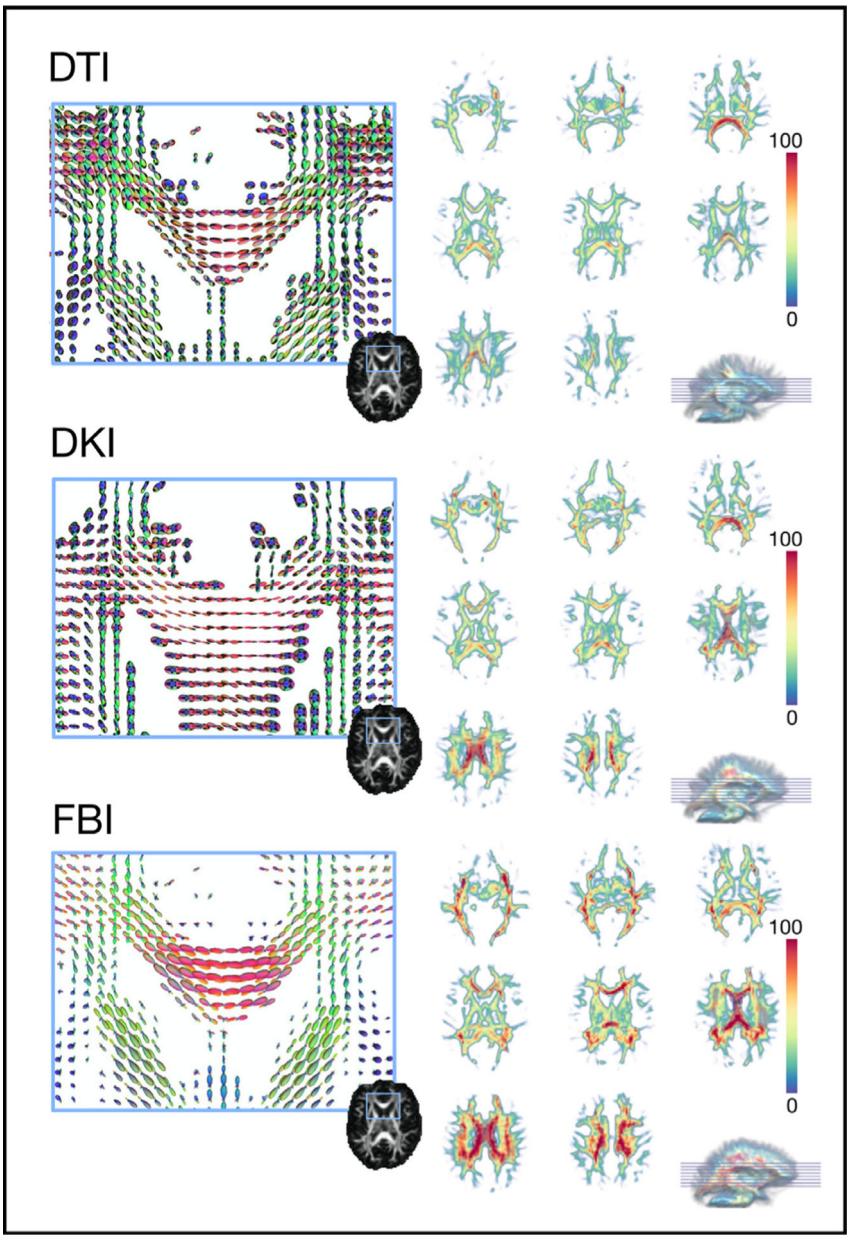


**Fig. 2. –.**

The ODFs obtained with each diffusion modality (DTI, DKI and FBI) are shown for the brain region corresponding to the blue inset in the axial slices. The same brain region is shown for all diffusion modalities. On the right side of each ODF magnification image, a mosaic demonstrating the tract density image from one representative subject is shown for each corresponding diffusion modality. The scale bar indicates the number of fibers per voxel.

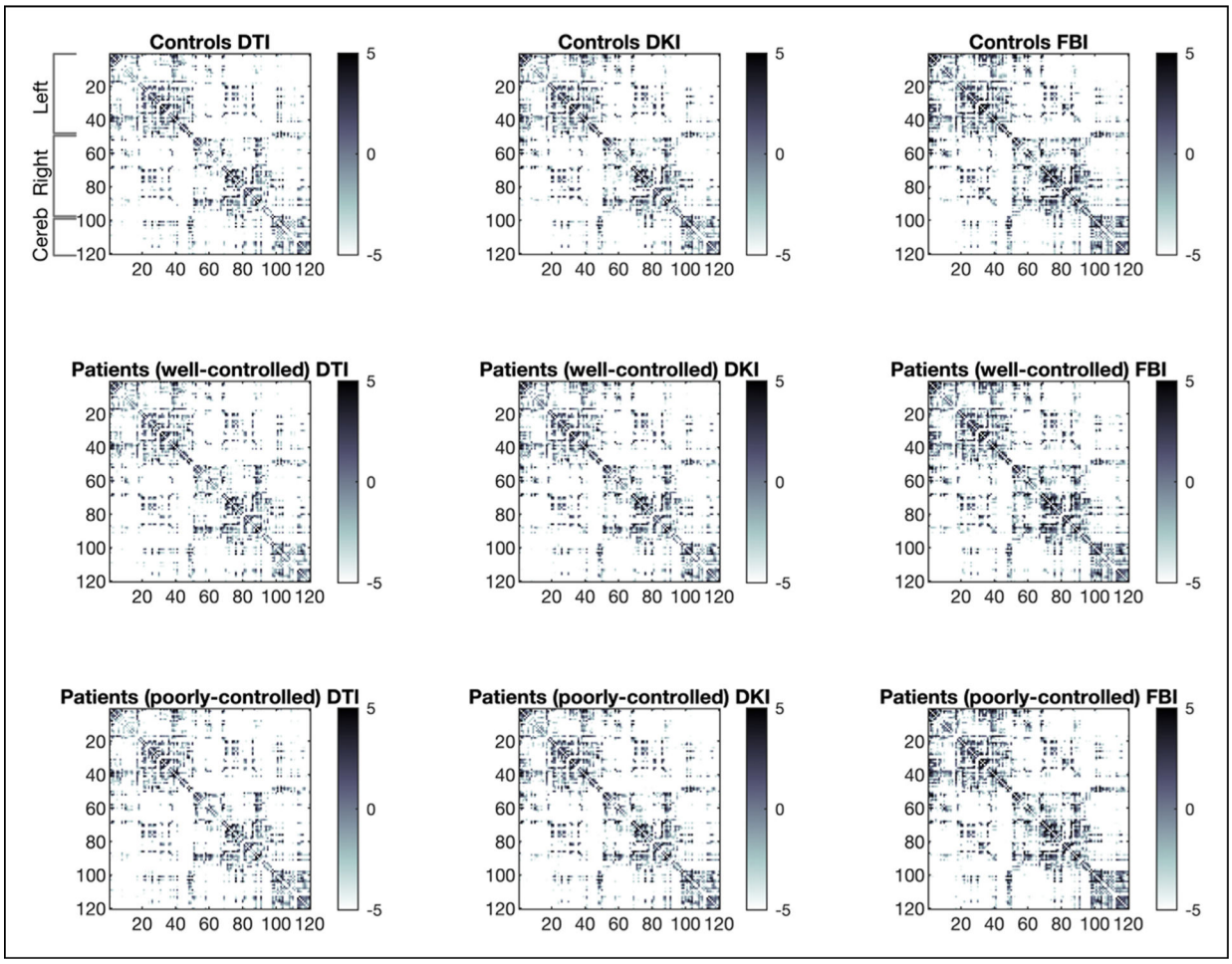


**Fig. 3. –.**

The group average whole brain connectome is shown for each diffusion modality. The ROIs in the connectome adjacency matrix are ordered in rows and columns in accordance with the AAL2 brain atlas, organized into left brain hemisphere, right brain hemisphere and cerebellum. The scale bars indicate the log(number of fibers normalized by the sum of the inverse of the length of their connections).

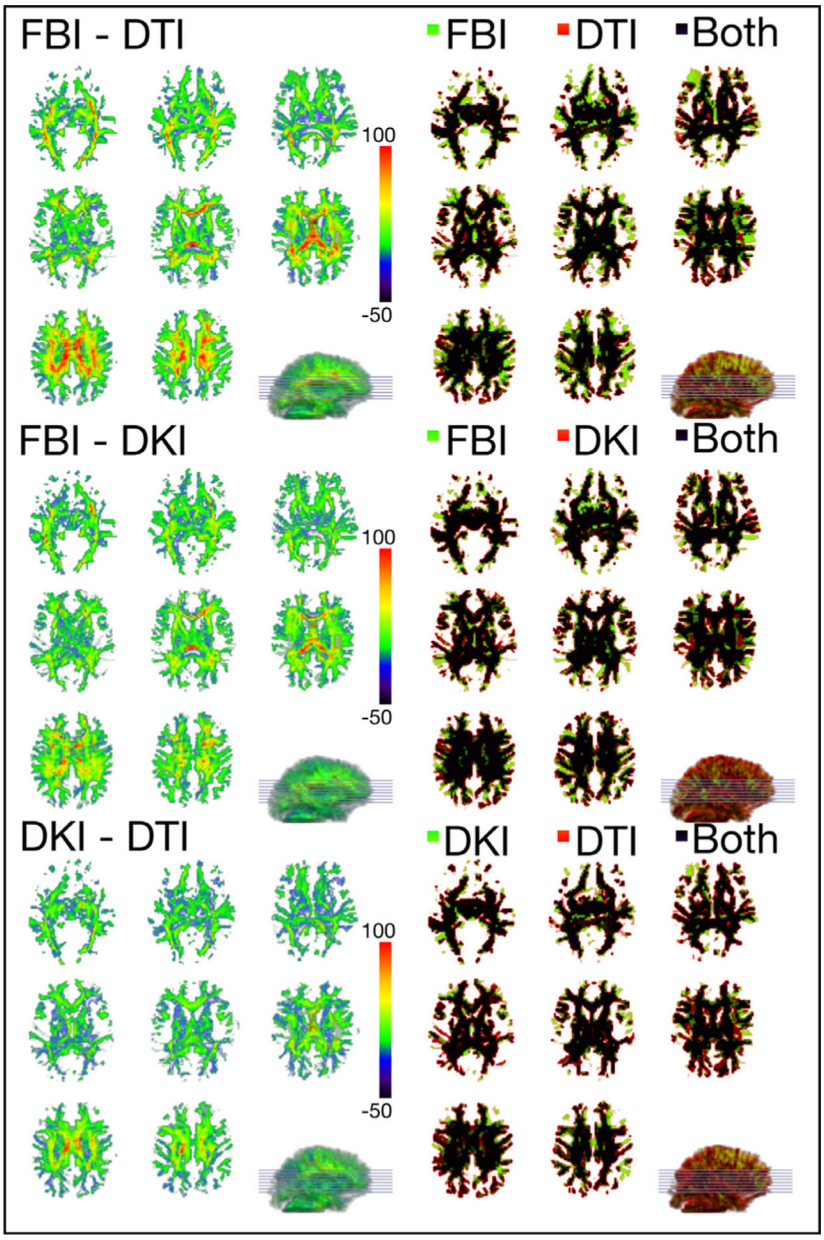


**Fig. 4. –.**

The left side mosaics demonstrate the absolute number of fibers tracked by each diffusion modality compared with another (subtraction). The scale bars indicate the absolute number of fibers per voxel. The right sided mosaics indicate voxels in which each modality was able to resolve 1 or more fibers.

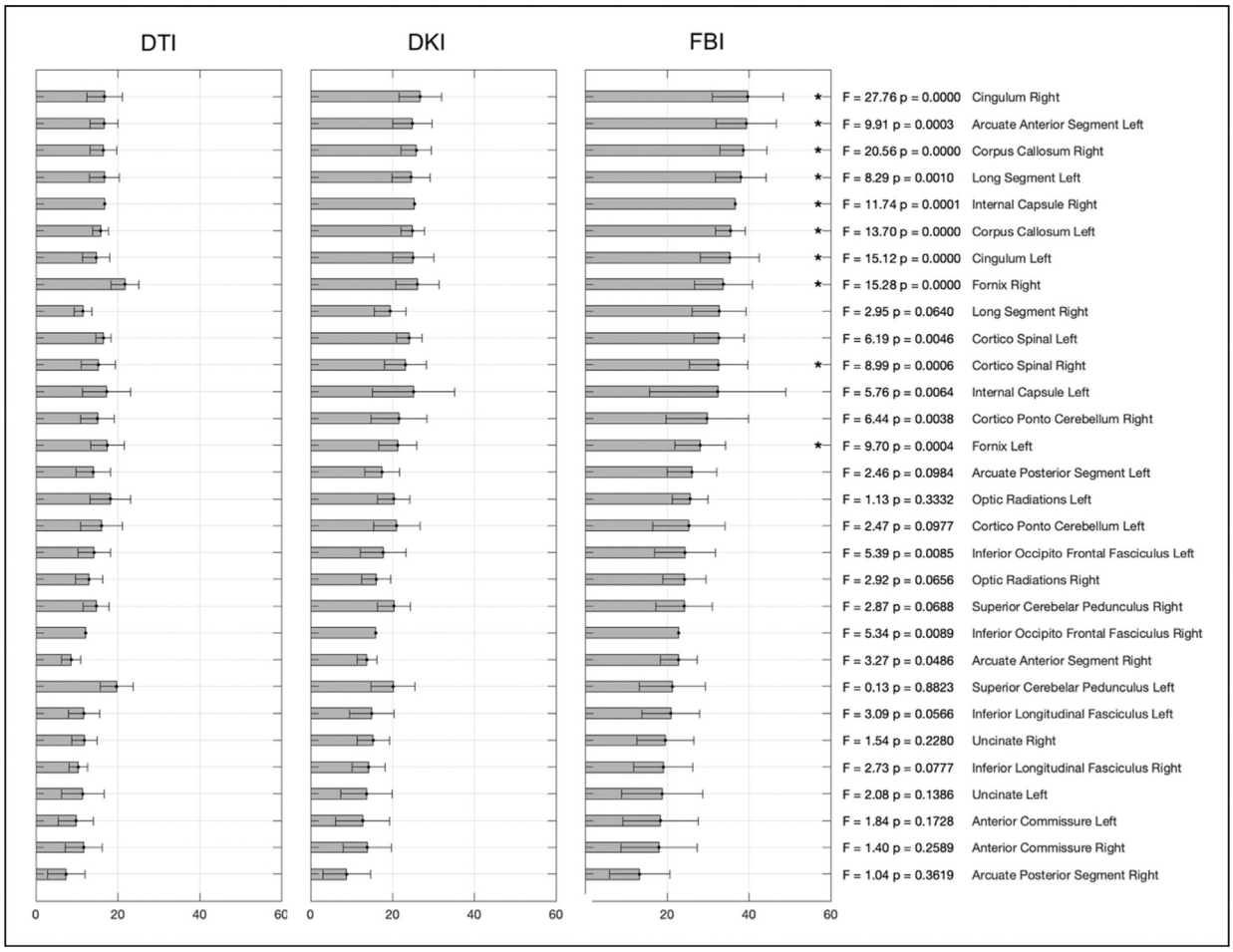


**Fig. 5. -**

Average number of fibers tracked per voxel (x-axis) in each white matter ROI from the NatBrainLab atlas across the three different diffusion modalities. The results of the one-way ANOVA for each ROI are shown on the right side for each ROI. Stars indicate significant group-wise differences corrected for multiple comparisons using Bonferroni.

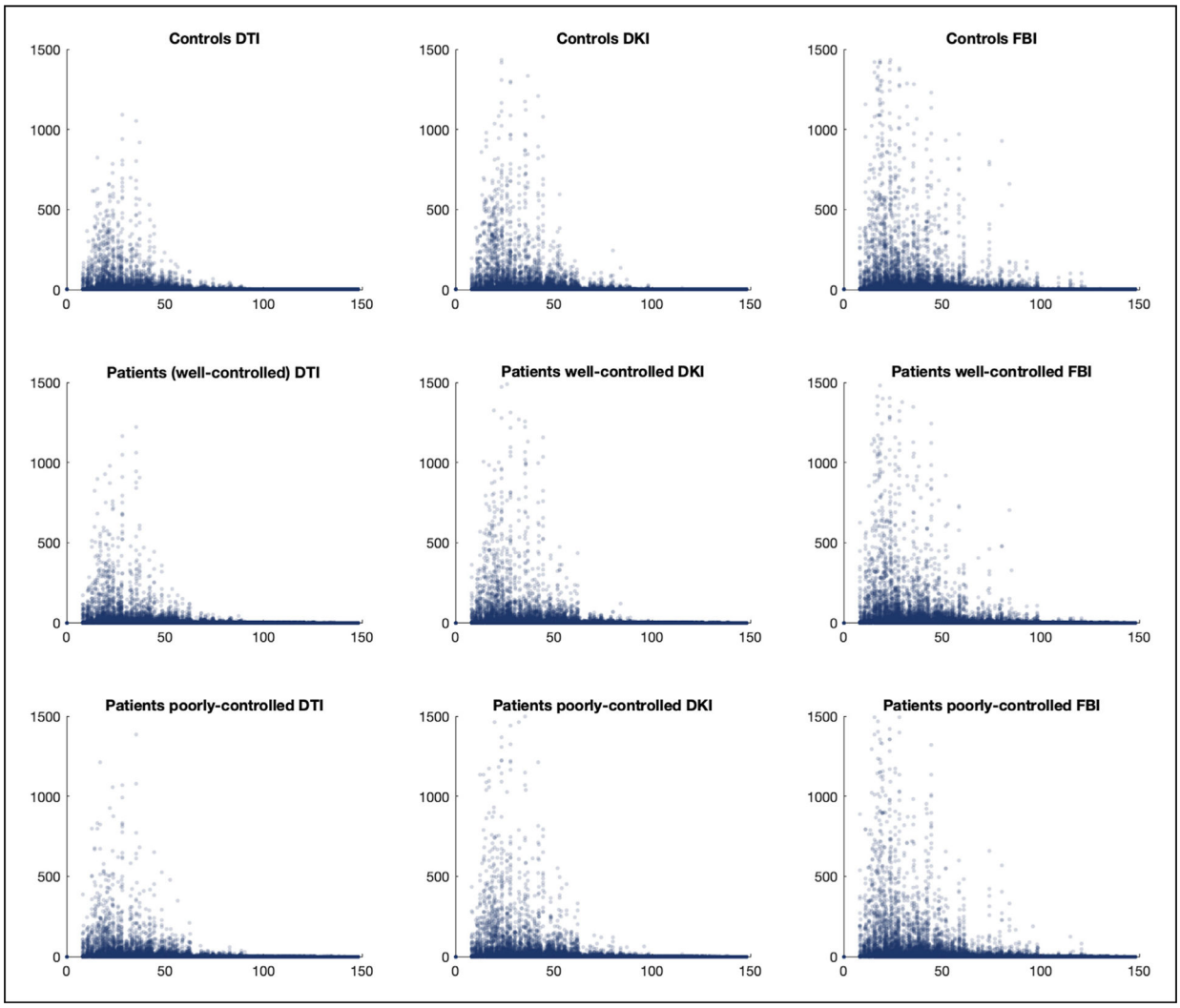


**Fig. 6. –.**

This scatter plot demonstrates the relationship between the average number of fibers tracked (x-axis) for each connectome link in relationship with the Euclidean distance in mm between the gray matter ROIs in the same link (y-axis).

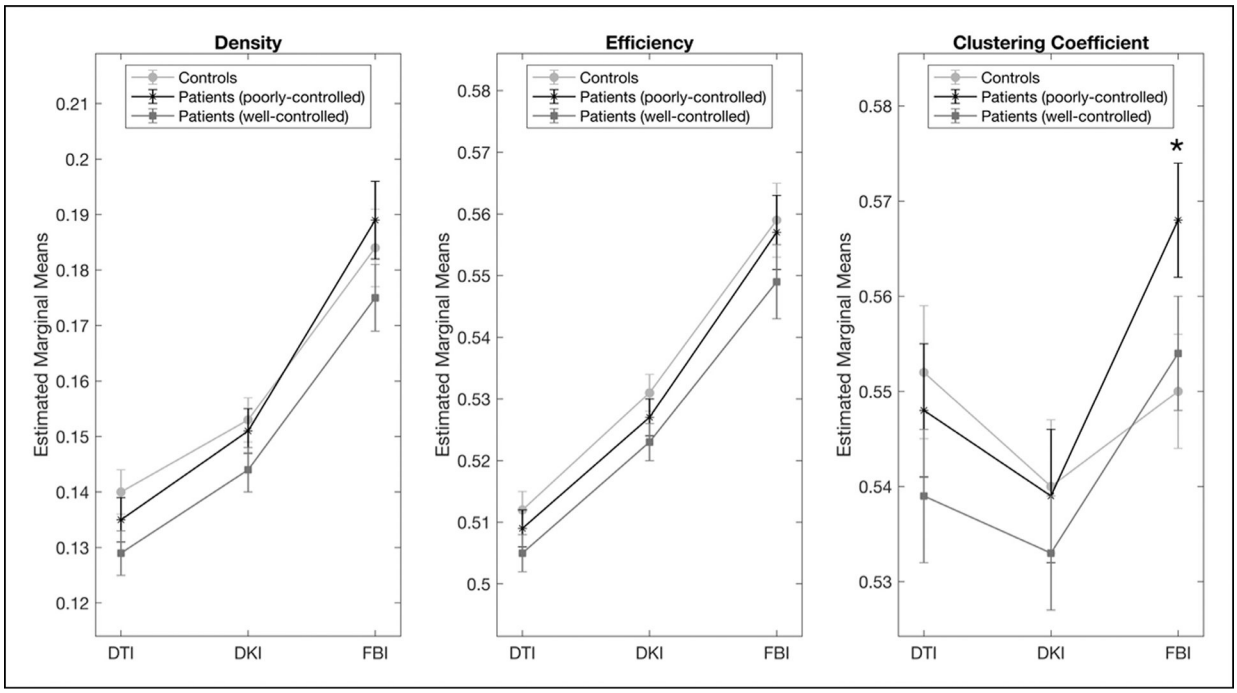


**Fig. 7. –.**

Error bar graphs demonstrating whole brain network properties. For all network measures, there was a significant within-subjects effect of diffusion modality. A significant interaction was observed between diffusion modality and subject group for global clustering coefficient, with a significantly higher global clustering coefficient observed in patients with poorly controlled epilepsy compared with controls.

*Neuroimage*. Author manuscript; available in PMC 2022 March 01.

**Table 1**

Demographic and clinical information per participant.

| Patient | Age at evaluation (years) | Gender | Handedness | Patient Group | Age at onset (years) | Presumed Onset Localization | Sz Freq.* | Seizure Type | Febrile Seizures | Medications |
|---|---|---|---|---|---|---|---|---|---|---|
| 1 | 33 | M | R | PC | 16 | L Frontal | 2 | FBTC | N | LEV 3250mg |
| 2 | 21 | F | L | PC | 1.5 | L Frontal | 20 | FIAS | Y | ZNS 500 mg, OXC 1600 mg, CLB 10mg |
| 3 | 34 | M | R | PC | 13 | PL Frontal | 1–2 | FBTC | N | LTG 125 mg VPA 2000mg |
| 4 | 18 | M | R | PC | 10 | L Frontal | 6 | FIAS | N | VPA 1000 mg, PHT 250mg |
| 5 | 51 | M | R | PC | 14 | Poorly Localized | 12 | FAS | Y | LEV 2000 mg, LTG 600mg |
| 6 | 26 | M | R | WC | 24 | Poorly Localized | 1–2 | FAS & FIAS | N | LTG 150mg |
| 7 | 48 | F | R | WC | 12 | L Temporal | 0 | FAS & FIAS | N | LTG 250mg |
| 8 | 50 | F | R | PC | 18 | Poorly Localized | 3–6 | FAS | N | LTG 600mg |
| 9 | 32 | M | L | PC | 23 | L Temporal | 1–2 | FAS | N | PHT 350 mg, VPA 1800mg |
| 10 | 51 | F | R | PC | 11 | L Temporal | 14 | FAS | N | CBZ 1000mg |
| 11 | 24 | F | R | WC | 21 | Poorly Localized | 0 | FAS | N | |
| 12 | 36 | F | L | PC | 20 | L Temporal | 15 | FAS & FIAS | N | BRV 100 mg, LCS 250 mg CLB 30mg |
| 13 | 38 | F | R | PC | 17 | L Frontoparietal | 16–20 | FBTC | N | ZNS 200 mg, LTG 600 mg, CLB 40mg |
| 14 | 48 | F | R | PC | 10 | R Temporal | 60 | FBTC | N | LEV 2000mg |
| 15 | 41 | F | R | PC | 27 | Unknown | 30–48 | FBTC | N | OXC 800mg |
| 16 | 33 | M | R | WC | 29 | L Poorly Localized | 0 | FBTC | N | VPA 1400mg |
| 17 | 28 | M | R | PC | 13 | L Temporal | 1 | FIAS | N | |
| 18 | 46 | F | R | WC | 22 | L Temporal | 4 | FAS & FIAS | N | OXC 900 mg, LTG 500 mg, LEV, 1000 mg, CLB 20 g |
| 19 | 60 | M | R | WC | 56 | Unknown | 1 | FAS & FIAS | N | LTG 300mg |
| 20 | 38 | F | R | WC | 30 | R Temporal | 0 | FBTC | Not known | LTG 175mg |
| 21 | 58 | F | L | PC | 11 | L Temporal | ~35 | FIAS | N | CLB 10 mg, LTG 200 mg, ZNS 300mg |
| 22 | 44 | M | R | WC | 39 | R Frontal | 0 | FBTC | N | OXC 1000 mg, LEV 2500 mg, CLB 10mg |
| 23 | 26 | M | R | WC | 21 | PL Temporal | 0 | FAS & FIAS | N | LTG 100mg |
| 24 | 29 | F | R | WC | 22 | L Temporal | 0 | FBTC | N | LTG 75mg |

| Patient | Age at evaluation (years) | Gender | Handedness | Patient Group | Age at onset (years) | Presumed Onset Localization | Sz Freq.* | Seizure Type | Febrile Seizures | Medications |
|---|---|---|---|---|---|---|---|---|---|---|
| 25 | 35 | M | R | WC | 31 | PL Frontal | 0 | FBTC | N | LTG 150mg |
| 26 | 59 | F | R | WC | 54 | Unknown | 1 | FBTC | Y | LEV 1000mg |
| 27 | 54 | M | R | WC | 43 | L Temporal | 2 | FBTC | Y | LEV 1000mg |
| 28 | 51 | F | R/L | WC | 48 | R Frontal | 3 | FBTC | N | LTG 100mg |
| 29 | 38 | F | R | WC | 36 | R Temporal | 2 | FBTC | N | LTG 200mg |

*F* = Female; *M* = Male; *R* = Right; *L* = Left; PL = Poorly Lateralized; WC = Well-Controlled; PC = Poorly-Controlled; FAS = Focal Aware Seizure; FIAS = Focal Impaired Awareness Seizure; FBTC = Focal to Bilateral Tonic-Clonic Seizure; *N* = No; *Y* = Yes; BRV = brivaracetam, CBZ = carbamazepine, CLB = clobazam; LEV = levetiracetam, LTG = lamotrigine, OXC = oxcarbazepine, PHT = phenytoin, VPA = valproic acid, ZNS = zonisamide;

*Seizure frequency at the time of last assessment (for well-controlled patients, the value reflects the frequency prior to achieving seizure freedom).

Of note, seizure types listed represent the event types experienced at time of assessment or at the last visit before seizure control was achieved on medication.